The Company of Biologists

RESEARCH ARTICLE

Proliferation-independent role of NF2 (merlin) in limiting biliary morphogenesis

Samira Benhamouche-Trouillet[1,2,3,*], Evan O'Loughlin[1,2,3,*], Ching-Hui Liu[1,2,3], William Polacheck[4], Julien Fitamant[1], Mary McKee[5], Nabeel El-Bardeesy[1], Christopher S. Chen[4] and Andrea I. McClatchey[1,2,3,‡]

ABSTRACT

The architecture of individual cells and cell collectives enables functional specification, a prominent example being the formation of epithelial tubes that transport fluid or gas in many organs. The intrahepatic bile ducts (IHBDs) form a tubular network within the liver parenchyma that transports bile to the intestine. Aberrant biliary 'neoductulogenesis' is also a feature of several liver pathologies including tumorigenesis. However, the mechanism of biliary tube morphogenesis in development or disease is not known. Elimination of the neurofibromatosis type 2 protein (NF2; also known as merlin or neurofibromin 2) causes hepatomegaly due to massive biliary neoductulogenesis in the mouse liver. We show that this phenotype reflects unlimited biliary morphogenesis rather than proliferative expansion. Our studies suggest that NF2 normally limits biliary morphogenesis by coordinating lumen expansion and cell architecture. This work provides fundamental insight into how biliary fate and tubulogenesis are coordinated during development and will guide analyses of disease-associated and experimentally induced biliary pathologies.

KEY WORDS: NF2, Merlin, ERM proteins, Bile duct morphogenesis, Lumen, Apical constriction, Mouse

INTRODUCTION

The coordinated establishment of polarity and communication among cells patterns epithelial tissues and can actively govern cell fate (Bryant and Mostov, 2008; Stephenson et al., 2010; Korotkevich et al., 2017). Precise and dynamic regulation of this coordination also enables epithelial tissue homeostasis and repair (Ishibe and Cantley, 2008; Nelson, 2009; Ragkousi and Gibson, 2014). Disease pathologies, including cancer, often reflect the unscheduled or ectopic re-enactment of morphogenetic processes, necessitating a deep understanding of their underlying cellular mechanisms (Muthuswamy and Xue, 2012; Macara and McCaffrey, 2013).

The highly regenerative liver is composed largely of two intimately related but architecturally distinct epithelial cell types: biliary epithelial cells and hepatocytes (Raynaud et al., 2011; Zong and Stanger, 2011; Kopp et al., 2016). Biliary epithelial cells organize radially around a central apical lumen to form tubules that constitute

the intrahepatic bile ducts (IHBDs). This tubular network is surrounded by hepatocytes that align in cords and establish apical lumens as canalicular channels within their lateral cell-cell junctions; these hepatic canaliculi align and drain into the IHBD tree. In the developing embryo both cell types are derived from a common precursor, the hepatoblast, and mounting evidence indicates that plasticity between the two differentiated cell types occurs during regenerative or disease-associated conditions in the adult liver (Kopp et al., 2016). Importantly, a hallmark of biliary pathology associated with chronic disease or tumorigenesis is the organization of aberrant biliary cells into polarized structures that mimic features of normal bile ducts (Desmet, 2011; Raynaud et al., 2011). Such 'neoductulogenesis' is likely to recapitulate aspects of IHBD formation in the embryonic liver. However, it is not known how the transition to a biliary fate is coordinated with the morphogenetic changes required to form a system of biliary tubes, largely owing to a lack of understanding of the earliest stages of this complex process.

Elimination of the neurofibromatosis type 2 protein (NF2; also known as merlin or neurofibromin 2) in the liver yields hepatomegaly in adult mice that is caused by massive biliary neoductulogenesis (Benhamouche et al., 2010; Zhang et al., 2010). NF2 is a classic tumor suppressor, the loss of which is associated with multiple human tumor types and has been linked to overproliferation caused by a number of signaling pathways (Petrilli and Fernandez-Valle, 2016). However, NF2 is a unique type of tumor suppressor that predominantly localizes to the plasma membrane-cytoskeleton interface and shares a close evolutionary and functional relationship with the membrane-cytoskeleton linking ERM (ezrin, radixin, moesin) proteins (Fehon et al., 2010). Indeed, many studies suggest that NF2, like the ERMs, has a fundamental role in organizing the membrane-cytoskeleton interface; as such, loss of NF2 alters fundamental properties of individual cells such as their polarity, mitotic spindle-to-cortex attachment and cortical cytoskeleton tension, as well as collective cellular behaviors including cell-cell communication, migration and lumen formation (Lallemand et al., 2003; Gladden et al., 2010; Hebert et al., 2012; Chiasson-MacKenzie et al., 2015; Das et al., 2015; Inaba et al., 2017).

To understand the basis of the striking biliary expansion caused by loss of NF2 in mice, we traced its origin. Our studies identify a proliferation-independent requirement for NF2 in the earliest stages of IHBD formation in the developing liver, and elucidate a novel self-organizing model of IHBD formation that will provide a valuable foundation for analyzing other developmental mutants and for understanding and manipulating plasticity under conditions of regeneration and disease in the adult liver.

RESULTS

Nf2 deletion yields biliary expansion without proliferation

Deletion of *Nf2* in the developing mouse liver yields hepatomegaly in adult mice, which is not due to the unscheduled proliferation of

[1]Massachusetts General Hospital Cancer Center, Charlestown, MA 02129, USA. [2]Harvard Medical School, Boston, MA 02114, USA. [3]Molecular Pathology, Massachusetts General Hospital, Charlestown, MA 02129, USA. [4]Department of Biomedical Engineering, Boston University, Wyss Institute, Boston, MA 02115, USA. [5]Center for Systems Biology, Program in Membrane Biology, Division of Nephrology, Department of Medicine, Massachusetts General Hospital and Harvard Medical School, Boston MA 02114, USA.
*These authors contributed equally to this work

‡Author for correspondence (mcclatch@helix.mgh.harvard.edu)

A.I.M., 0000-0002-6150-3619

DEVELOPMENT

1

hepatocytes but rather to the massive expansion of biliary-like cells and neoductulogenesis surrounding the portal endothelial tree throughout the liver (Benhamouche et al., 2010; Zhang et al., 2010). This phenotype resembles the more limited 'ductular reactions' that occur in the diseased human liver or in response to experimentally induced injury in rodents (Preisegger et al., 1999; Akhurst et al., 2001; Richardson et al., 2007; Bioulac-Sage and Balabaud, 2010).

Liver-specific conditional deletion of *Nf2* in *Alb-Cre;Nf2^lox/lox* (*Nf2^cKO*) mice begins as early as embryonic day (E) 9.5 and yields excess biliary structures that are already apparent at birth, suggesting that the phenotype initiates during development (Benhamouche et al., 2010). IHBD formation in the embryonic liver is initiated at ~E14.5-E15.5 by periportal hepatoblasts, referred to as ductal plate cells, that are induced to express the biliary marker Sox9 by neighboring portal endothelial cells (Raynaud et al., 2011; Zong and Stanger, 2011). This is followed by a poorly understood process of tubulogenesis that creates a biliary tree that is congruent with that of the portal endothelium (Antoniou et al., 2009; Zong et al., 2009; Carpentier et al., 2011; Poncy et al., 2015). To determine whether biliary expansion in the *Nf2^cKO* liver initiates during IHBD morphogenesis, we monitored the number and distribution of Sox9+ cells in developing *Nf2^cKO* and control (*Nf2^lox/lox*) embryonic livers (Fig. 1A). As expected, periportal Sox9+ ductal plate cells were present by E15.5 in control livers at the onset of IHBD formation (Fig. 1A). Quantification of the number of Sox9+ cells per portal circumference for all portals that were in cross-section (see Materials and Methods) revealed that *Nf2^cKO* and control livers exhibited similar numbers and distribution of Sox9+ cells at E15.5-E16.0 (Fig. 1A,B). However, beginning at E16.5, a progressive and dramatic increase in periportal Sox9+ cells was evident in *Nf2^cKO* livers (Fig. 1A,B, Fig. S1A). In postnatal *Nf2^cKO* livers, supernumerary Sox9+ cells formed still-expanding periportal nests of polarized lumen-containing structures that resembled enlarged, misshapen IHBDs (Fig. 1A).

We next asked whether proliferation contributes to the dramatic expansion of Sox9+ cells in the developing *Nf2^cKO* liver. The overall size of embryonic control and *Nf2^cKO* livers was similar (not shown) and proliferating Sox9− cells were evident outside of the periportal area in both control and *Nf2^cKO* livers from E15.5 to postnatal day (P) 2, but declined thereafter such that few dividing cells were detectable in later postnatal or adult livers of either genotype (Fig. 1C). Surprisingly, however, very few if any dividing Sox9+ biliary cells were present in control or *Nf2^cKO* livers through P9 (Fig. 1C, Fig. S1B). Therefore, the substantial increase in Sox9+ cell number that occurs in the absence of the NF2 tumor suppressor reflects the unregulated induction of biliary morphogenesis without cell division. Notably, in 6- to 8-week-old *Nf2^cKO* livers, but not in controls, dividing Sox9+ cells were readily detected within the expanding neoductular lesions, suggesting a second stage of growth (Benhamouche et al., 2010).

Increased recruitment of cells to immature biliary structures in the absence of NF2

In the developing *Nf2^cKO* liver, excess Sox9+ cells were restricted to periportal areas and neither ectopic Sox9+ cells nor IHBDs were found in the parenchyma (Fig. S1C). In addition, the density and distribution of cells expressing HNF4α, a marker of developing hepatocytes, which represent the vast majority of cells in the embryonic and adult liver, was similar in *Nf2^cKO* and control livers, and excess Sox9+ cells in the *Nf2^cKO* livers did not maintain HNF4α expression (Fig. S1D,E). These data suggest that NF2 deficiency triggers the over-recruitment of cells to a biliary fate due to a failure to limit the normal process of IHBD formation.

The early stages of IHBD formation in the normal developing liver are poorly understood. The induction of Sox9 expression by periportal ductal plate cells is rapidly followed by the appearance of clusters of Sox9+ cells that form polarized structures surrounding a central lumen (Zong and Stanger, 2011). This process involves the recruitment of Sox9− HNF4α+ cells from the surrounding parenchyma to form asymmetric primitive ductular structures (PDSs), which are converted into symmetric structures in which all cells are Sox9+ HNF4α− (Antoniou et al., 2009; Zong et al., 2009). Increased Sox9+ biliary cells in the developing *Nf2^cKO* liver could reflect an increase in the number of polarized Sox9+ structures and/or in the number of Sox9+ cells recruited to each structure (Fig. 2A). We found that ERM proteins, which are closely related to NF2, and their binding partner Na+/H+ exchanger regulatory factor 1 (NHERF1; also known as SLC9A3R1), strongly mark the apical surfaces of cells in immature Sox9+ biliary structures as they are forming around each portal vein, allowing us to distinguish between these possibilities (Fig. 2B) (Fehon et al., 2010). We noted that in control livers the total number of Sox9+ cells scales with portal circumference in addition to embryonic stage, owing to an increase in the number of polarized biliary structures per portal space and in the number of Sox9+ cells associated with each structure, respectively; these relationships were particularly evident at E18.5, when a variety of portal diameters and IHBD stages coexist (Fig. 2C, Fig. S2A,B). Closer inspection of control livers revealed that the number of Sox9+ immature biliary structures per portal space declined after P2 until only one to two mature bile ducts per portal space remained in the adult (Fig. 2D, Fig. S2C). Consistent with other studies, we did not detect cell death within the polarized structures (Carpentier et al., 2011); instead, many seemed to 'regress', losing apicobasal polarity and converting to a hepatocyte fate and architecture (Fig. S2D, Fig. S5C). Moreover, the number of cells associated with each polarized structure plateaued before birth, was independent of portal size and was the same as the average number of cells surrounding mature bile ducts in the adult liver (Fig. 2E). Therefore, the morphogenetic process that assembles biliary structures *de novo* and without proliferation in the normal developing liver includes a mechanism for 'counting' the optimal number of cells that are assembled to form the tube circumference that is maintained in the adult.

Nf2^cKO livers initiated the same number of immature biliary structures (Fig. 2D); however, the number of Sox9+ cells per polarized structure accumulated significantly (Fig. 2E). Moreover, the number of polarized structures did not decline in the *Nf2^cKO* liver, indicating a failure of these structures to 'regress' (Fig. 2D). Thus, NF2 is required for the 'counting' mechanism that determines biliary tube circumference; enlargement of the biliary tube may, in turn, impair the normal regression of polarized structures that instills the final optimal architecture of the biliary tree.

De novo polarization and lumen formation initiate biliary morphogenesis

We defined presumptive stages in the formation of polarized biliary structures in control livers based on the number of Sox9+ cells in each and their frequency with respect to embryonic age and increasing portal size (Fig. 3). Antibodies that detect phosphorylated, activated ERMs (pERM), NHERF1 and moesin/radixin but not ezrin (see Materials and Methods) (Saotome et al., 2004) similarly marked all stages (Fig. 3, Fig. S3A,B). This analysis uncovered several novel aspects of the coordination of cell fate and morphogenesis during this process.

First, IHBD formation is initiated by the *de novo* polarization of a single cell. At the earliest stages, rather than a continuous 'sleeve' of
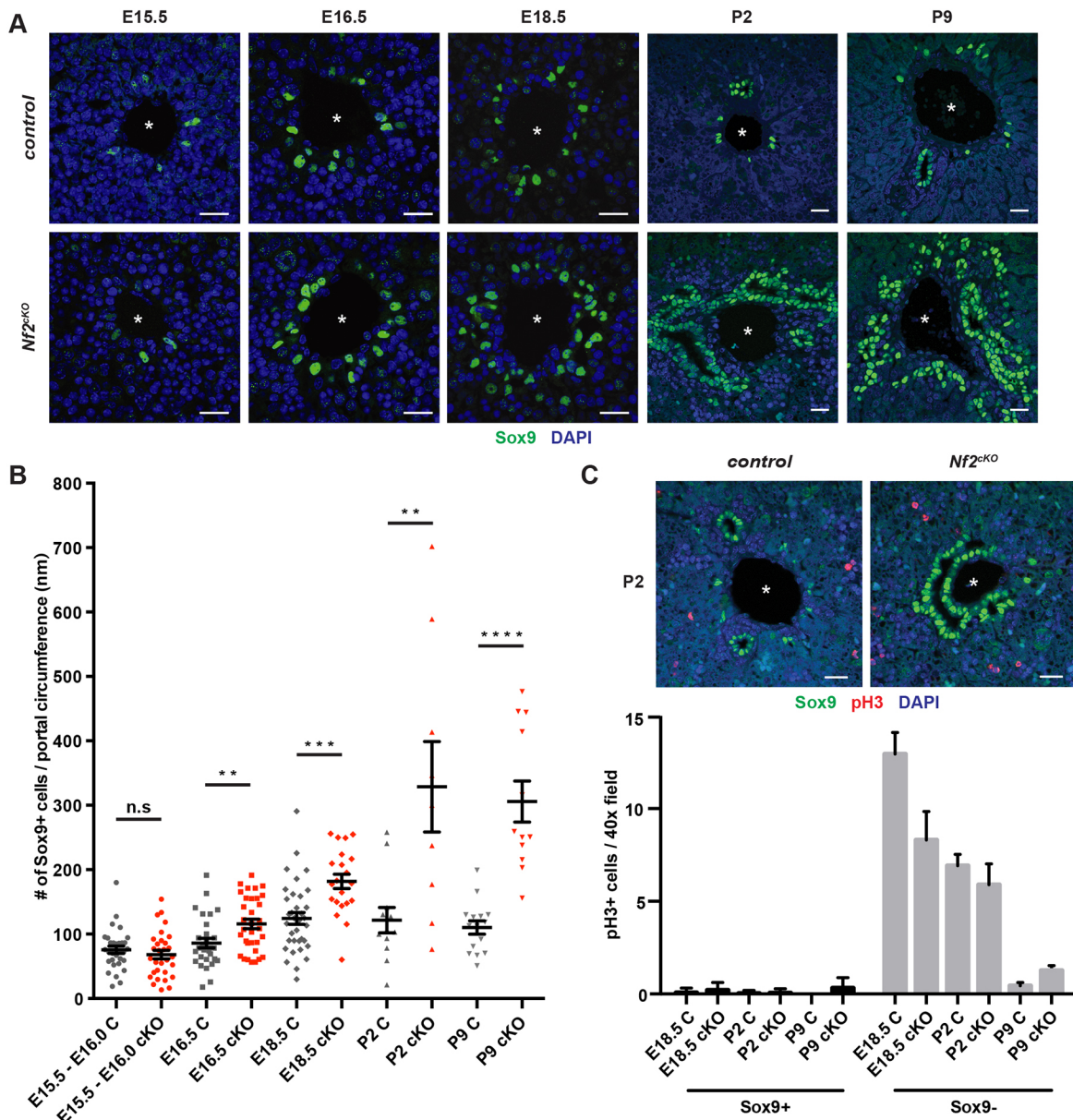
Fig. 1. Proliferation-independent expansion of biliary cells in the embryonic *Nf2^{cKO}* liver. (A) Representative confocal images showing the number and distribution of Sox9$^+$ (green) cells in control and *Nf2^{cKO}* mouse livers at E15.5, E16.5, E18.5, P2 and P9. Portal veins are marked by asterisks. (B) Quantitation of the number of Sox9$^+$ cells per portal circumference at the specified stages. n.s, not statistically significant; **$P<0.01$, ***$P<0.001$, ****$P<0.0001$ (Student's *t*-test). Each data point represents an individual portal space. Sample sizes [control (C), *Nf2^{cKO}* (cKO) embryos]: E15.5-E16.0 (9, 10), E16.5 (12, 5), E18.5 (10, 5), P2 (4, 3), P9 (4, 2). (C) Sections from P2 control and *Nf2^{cKO}* livers stained for Sox9 and pH3 (top), along with a quantitation of proliferating (pH3$^+$) Sox9$^+$ and Sox9$^-$ cells (bottom). Values are mean±s.e.m. Sample sizes (control, *Nf2^{cKO}* embryos): E18.5 (3, 4), P2 (3, 3), P9 (2, 2). Scale bars: 20 µm.

Sox9$^+$ cells surrounding the portal endothelium, individual Sox9$^+$ cells were common and always associated with a strong, isolated punctum of ERM/NHERF1 that localized specifically to a cell-cell boundary distal to the endothelium (Fig. 3, stage 1; Fig. S3C).

Second, our analyses strongly suggest that the expansion of Sox9$^+$ cells within polarized structures occurs via an inductive process that involves cell-cell communication and coordinated lumen expansion. Individual polarized Sox9$^+$ cells progress to Sox9$^+$ doublets, which are always associated with an ERM/NHERF1$^+$ punctum or, frequently, an expanded area of ERM/NHERF1$^+$ membrane (Fig. 3, stage 2). By E18.5, larger contiguous clusters of Sox9$^+$ cells are frequent and associated with expanded ERM/NHERF1 surface (stage 3) that surrounds an increasingly

open luminal space (stage 4). As has been described, cells on the parenchymal side of these PDSs are initially Sox9$^-$ (Antoniou et al., 2009; Zong et al., 2009). The simplest model to explain the conversion of PDSs to symmetric structures harboring an open lumen encircled completely by Sox9$^+$ cells (Fig. 3, stage 5) invokes the sequential radial induction of Sox9 via cell-cell contact, since Sox9$^+$ cells always contact at least one other Sox9$^+$ cell. Importantly, at every stage, neighboring Sox9$^-$ ductal plate or parenchymal cells (green striped cells in Fig. 3) that physically contact these ERM/NHERF1/Sox9$^+$ initiating cells are obligatory participants in the process of *de novo* lumen formation and expansion via the imposed conversion of their own cell contact into luminal surface, and they are therefore polarized relative to it. Since
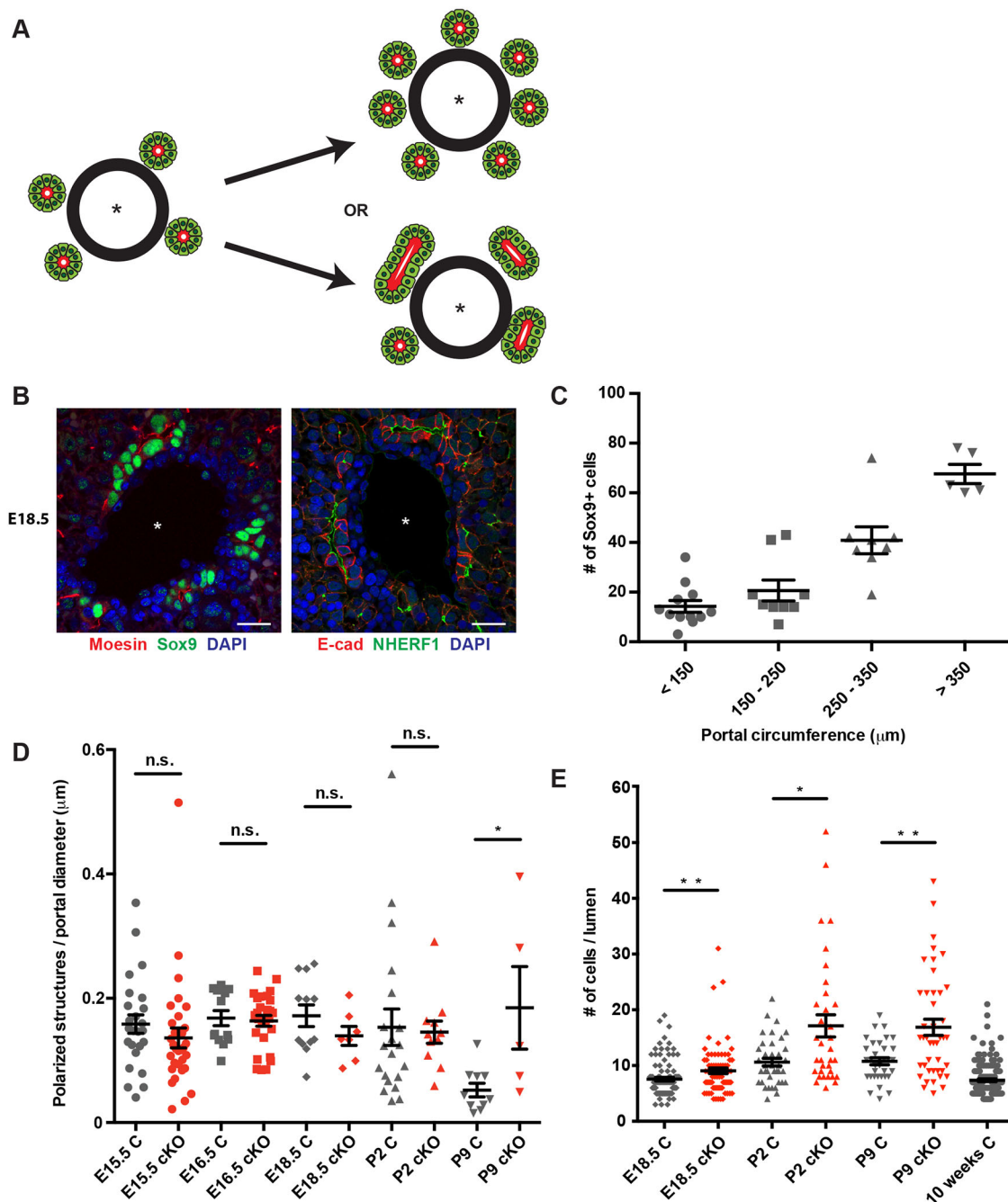
Fig. 2. Ectopic Sox9⁺ cells are recruited to each polarizing biliary structure in the absence of NF2. (A) Excess periportal Sox9⁺ cells in the *Nf2^cKO* liver could reflect an increase in the number of polarized structures that are initiated (top) or an increase in the number of Sox9⁺ cells that are recruited to each structure (bottom). Asterisk, portal vein. (B) Confocal images showing the localization of moesin (left) and NHERF1 (right) to the luminal surface of immature biliary structures in control E18.5 livers, allowing the identification of individual polarized structures. Scale bars: 20 μm. (C) Quantitation of the number of periportal Sox9⁺ cells as a function of portal circumference in the E18.5 control liver. *n*=10 control embryos evaluated. (D) Comparison of the number of individual polarized structures in the developing control (gray) and *Nf2^cKO* (red) liver normalized to portal diameter. Each data point represents an individual portal space. Sample size (control, *Nf2^cKO* embryos): E15.5 (5, 9), E16.5 (3, 4), E18.5 (4, 3), P2 (6, 4), P9 (4, 2). (E) Quantitation of the number of Sox9⁺ cells per polarized structure in control (gray) and *Nf2^cKO* (red) livers. Note that the number of Sox9⁺ cells per polarized structure in *Nf2^cKO* is an underestimate because many are shared between two polarized structures and were only counted once. Each data point represents one polarized structure. Sample size (control, *Nf2^cKO* embryos): E18.5 (4, 3), P2 (6, 4), P9 (4, 2), 10 weeks (3). (D,E) n.s., not statistically significant; *P<0.05, **P<0.01 (Mann–Whitney test). Values are mean±s.e.m.

these cells are destined to express Sox9, these observations are consistent with the idea that polarization and lumen formation 'primes' cells to adopt a biliary cell fate.

Third, the sequential expansion and then constriction of the apical surface contributes to IHBD morphogenesis. The initial expansion of ERM/NHERF1⁺ apical membrane along the jagged boundaries between ductal plate cells and adjacent parenchymal hepatoblasts is followed by a significant narrowing of the apical width of the cells, which acquire the characteristic wedge shape of cells that are organized radially around an open lumen in mature biliary structures (Fig. 3, stage 5). Remarkably, the number of cells forming the circumference of each biliary structure at this stage is similar (~8-14
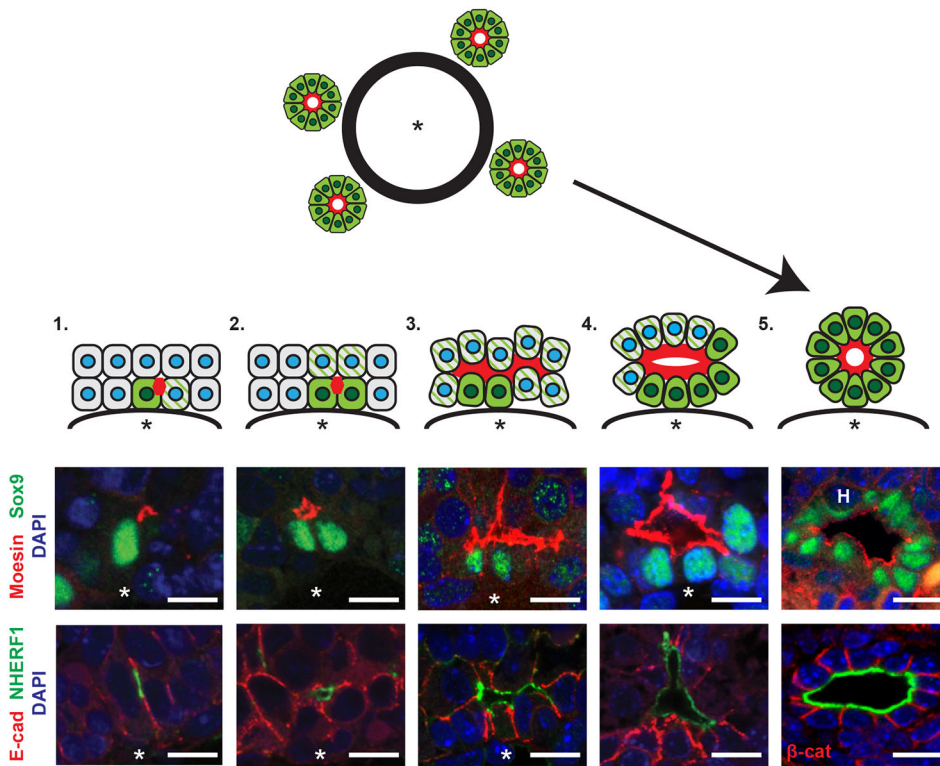
DEVELOPMENT

4

Fig. 3. Stages of *de novo* biliary morphogenesis. Interpretative diagram and matched images showing five presumptive stages of intrahepatic biliary duct formation in the normal developing liver. (1) Single Sox9+ cells (green) with associated moesin/NHERF1+ punctum (red) and neighboring, obligately polarized future Sox9+ cells (green striped). (2) Sox9+ doublet with moesin/NHERF1+ apical surface in between. (3) Three or more consecutive ductal plate cells associated with moesin/NHERF1+ apical surface, Sox9 expression and some apical constriction. (4) Primitive ductal structure with open lumen, asymmetric distribution of Sox9+ cells and more uniform apical constriction. (5) Complete ductal structure with patent lumen surrounded completely by wedge-shaped Sox9+ cells. Asterisk, portal vein. H, hematopoietic cell. Scale bars: 10 µm.

cells) regardless of portal diameter, and matches that of IHBDs in the adult liver (see Fig. 2E). This suggests that a mechanism that limits lumen expansion in coordination with apical constriction defines IHBD circumference. Together, these morphogenetic studies suggest that IHBD formation and the acquisition of biliary fate involves coordinated polarity induction, lumen expansion and apical constriction.

Ultrastructural analysis of developing IHBDs
To gain more insight into the earliest stages of IHBD morphogenesis, we examined portal spaces in E15.5-E16.5 livers ultrastructurally. The fetal liver is a major site of hematopoiesis at this stage (Mikkola and Orkin, 2006), and transmission electron microscopy (TEM) revealed a complex relationship between ductal plate cells and hematopoietic cells, which they often completely envelop (Fig. 4A). The number of periportal hematopoietic cells declines after E16.5, and it is not known whether they functionally contribute to the onset of IHBD morphogenesis (Mikkola and Orkin, 2006). TEM confirmed the existence of microlumens (~1 µm) between ductal plate cells that are filled with microvilli and flanked by electron-dense junctions (Fig. 4B). Expanded (~6 µm) microvillus-filled lumens were often observed in tandem along cell-cell boundaries and involved both ductal plate and overlying parenchymal cells (Fig. 4C). Microlumens were often adjacent to large cytoplasmic vesicles, suggesting an active process of apical surface expansion (Fig. 4D). In fact, some cell-cell boundaries harbored similar stretches of electron-dense junction and adjacent vesicles without microlumens, which might reflect the earliest step in the process, perhaps constituting the apical membrane initiation site (AMIS) described in 3D *in vitro* cysts (Fig. 4E) (Bryant et al., 2010). Finally, open lumens circumscribed by multiple cells were readily identified (Fig. 4F). Notably, microvilli were most dense in the smallest identifiable microlumens, in small expanding lumens and in pockets or

crevasses at the edges of partially open multicellular lumens, but were lost from the more mature expanded luminal surface (Fig. 4A-D,F). This was mirrored by the enrichment of ERMs, which are known to have crucial roles in the formation and function of microvilli (Fig. S4A) (Fehon et al., 2010). At all stages, lumens were demarcated by electron-dense junctions that had mixed features of tight and adherens junctions, consistent with the colocalization of ZO-1 (Tjp1) with E-cadherin at apical junctions in early polarized structures (Fig. S4B). The apical polarity marker Par3 (Pard3) and its regulator aPKC also localized along the developing apical surface at all stages (Fig. S4C,D), consistent with the *de novo* initiation and expansion of apical lumens during IHBD formation.

Aberrant morphogenesis of polarized biliary structures in the developing *Nf2^cKO* liver
Using our staging of normal biliary development as a guide, we examined the mechanism by which polarized structures in *Nf2^cKO* livers acquire excess Sox9+ cells. Inspection of E15.5-E18.5 *Nf2^cKO* livers by confocal imaging and TEM revealed that microlumens initiated with similar frequency, distribution and architecture as in control (Fig. 5A,B, Fig. S5A,B). However, *Nf2^cKO* livers exhibited an acceleration of stage 4-5 structures in the mutant beginning at E16.5 (Fig. 5B). We have shown previously that an important function of NF2 is to limit cortical ERM activity, and that NF2 deficiency causes the formation of ectopic ERM-positive apical lumens in 3D cyst cultures (Hebert et al., 2012; Chiasson-MacKenzie et al., 2015). Indeed, we found that, beginning at E16.5, polarized Sox9+ structures in *Nf2^cKO* livers exhibited an exaggerated expansion of ERM+ and NHERF1+ luminal membrane, which was associated with the incorporation of excess Sox9− cells into the polarized structure (Fig. 5C).

An additional consequence of increased cortical ERM activity in cultured NF2-deficient monolayers is unregulated medioapical
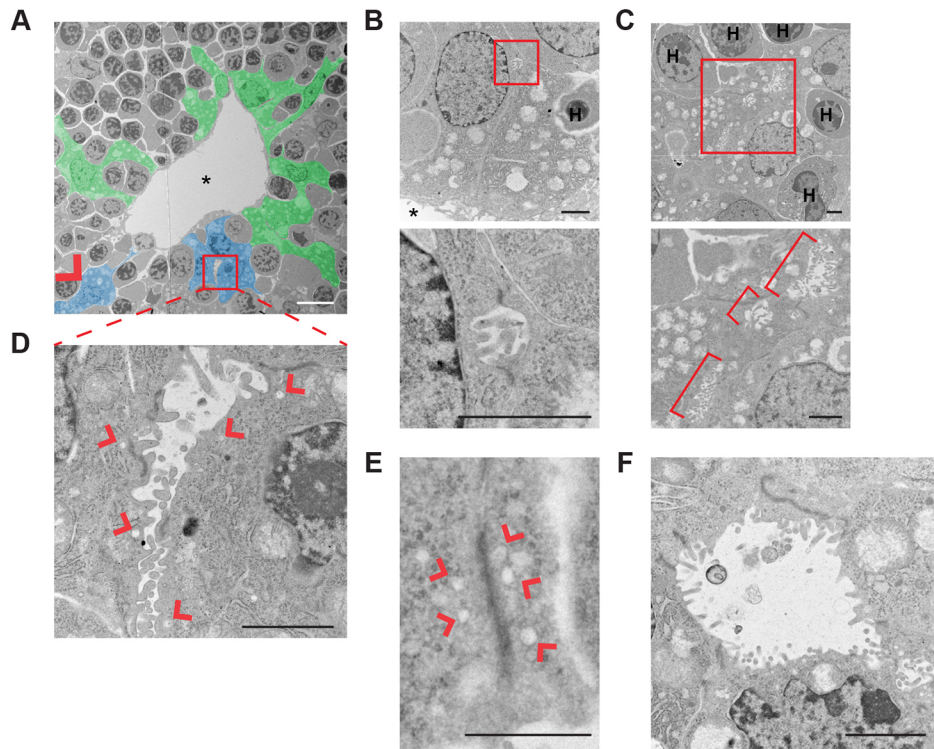
5

Fig. 4. Ultrastructural analysis of *de novo* lumen formation during biliary morphogenesis in control livers. (A) Transmission electron micrograph of a portal space in a control E15.5 liver pseudo-colored to show ductal plate cells (blue) that form microlumens flanked by electron-dense junctions (red box and arrowhead) along shared boundaries with parenchymal hepatoblasts (also blue) in this plane of section. Other ductal plate cells that do not form *de novo* lumens in this plane of section are shown in green; many envelop hematopoietic cells (gray surrounded by green). Portal vein is marked by an asterisk. (B-F) High-magnification of examples of developing luminal structures generated by ductal plate cells in control E15.5-E16.5 livers. Boxed areas (B,C) are magnified beneath. (B) Microlumen (~1 μm) filled with microvilli and flanked by electron-dense cell junctions formed at the ab-endothelial boundary between two ductal plate cells. (C) Tandem microlumens along boundaries between two ductal plate cells and one parenchymal hepatoblast (brackets). (D) Expanding lumen (2-6 μm) filled with microvilli and flanked by electron-dense cell junctions and associated vesicular structures (arrowheads). (E) Elongated electron-dense cell junction without microlumens but clearly associated with vesicular structures (arrowheads). (F) Open lumen with fewer microvilli surrounded by wedge-shaped cells that are connected by electron-dense apical junctions. H, hematopoietic cell. Scale bars: 10 μm in A; 2 μm in B-D,F; 1 μm in E.

tension, which is known to functionally regulate apical constriction *in vivo* (Martin and Goldstein, 2014; Chiasson-MacKenzie et al., 2015). Indeed, in contrast to the relatively homogeneous apical width exhibited by wild-type cells in stage 4+ IHBDs, apical width was highly variable in developing *Nf2^cKO^* IHBDs, with many cells exhibiting a several-fold increase in apical-to-basal surface ratio (Fig. 5D). This was accompanied by an increase in lumen opening (Fig. 5E).

Together, these observations are consistent with the possibility that the inappropriate coordination of lumen expansion and apical constriction leads to the over-recruitment of cells to developing IHBD structures. In addition, perhaps due to their enlargement, polarized structures did not regress in the *Nf2^cKO^* liver (see Fig. 2D), a phenomenon evident at P2 when 'dimmed', regressing structures are obvious in control but not *Nf2^cKO^* livers (Fig. S5C). Importantly, unabated neoductulogenesis in the postnatal *Nf2^cKO^* liver was associated with continuing lumen expansion and recruitment of Sox9⁻ cells, progressively limiting the number of normal hepatocytes available to support liver function and a likely cause of the death of many of these animals (Fig. 5F) (Benhamouche et al., 2010).

3D analysis of initiating lumens in embryonic wild-type and *Nf2^cKO^* livers

3D analysis underscored the complexity of early IHBD luminal architecture and provided further insight into how the lumen expands in the normal and mutant liver (Fig. 6A, Fig. S6A, Movie 1).

Evaluation of the luminal surface demarcated by NHERF1 staining revealed several key aspects of the shape of the expanding lumens at E16.5 prior to substantial apical constriction. First, lumens in the normal liver were nearly all prolate in shape, exhibiting little vertical extension along the portal vein and a dominant axis most often tangent to the portal circumference (Fig. 6B, Fig. S6B). By contrast, a significant fraction of the mutant lumens exhibited an oblate shape, despite having long axes of similar magnitudes to control, suggesting that they are less restricted in their expansion (Fig. 6B, Fig. S6C). Finally, as the lumens increased in size, the sphericity of the inner luminal cavities, measured as NHERF1 void volumes, declined in the control but not in the mutant, consistent with the increased lumen opening that we measured in two dimensions (Fig. 6C, Fig. 5E). The shape and limited vertical extension of the developing luminal structures is consistent with the likelihood that polarized biliary structures assemble *de novo*, and later expand and interconnect vertically to form a continuous tubular tree rather than expanding dendritically from existing biliary tree tips (Takashima et al., 2015).

DISCUSSION

Epithelial tubes are integral to the functional anatomy of many organs and form via either invagination of an existing epithelial monolayer into a tube that surrounds a central lumen or via the *de novo* formation of lumens and coordinated rearrangement of adjacent cells (Sigurbjörnsdóttir et al., 2014). One predominant form of *de novo* lumen formation, known as cord hollowing,
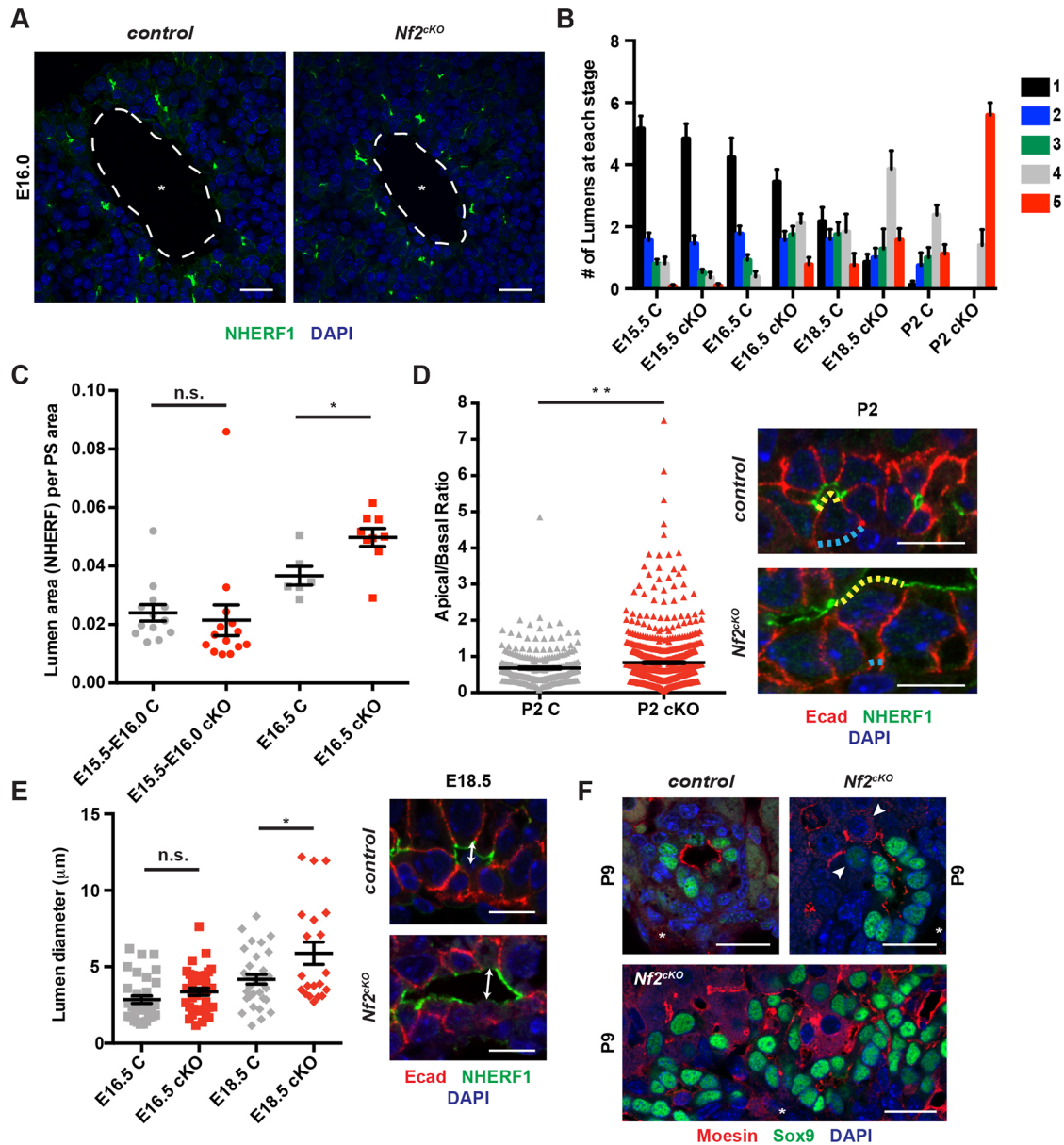
Fig. 5. Altered lumen expansion in the *Nf2^cKO* liver. (A) Representative confocal images of similarly sized NHERF1+ lumens in E16.0 control and *Nf2^cKO* livers. (B) Frequency of each IHBD stage (from Fig. 3) in control and *Nf2^cKO* livers of various ages. Sample size (control, *Nf2^cKO*): E15.5 (5, 9), E16.5 (3, 4), E18.5 (4, 3), P2 (6, 4). (C) Quantitation of NHERF1+ lumen surface in control and *Nf2^cKO* livers at E15.5-E16.5. PS, portal space. n.s., not statistically significant; *P<0.05 (Student's unpaired t-test). Each data point represents one lumen surface. Sample size (control, *Nf2^cKO*): E15.5-E16.0 (4, 3), E16.5 (5, 3). (D) Variation of apical width [ratio of apical (yellow dotted line in representative confocal images) to basal (blue dotted line) width] in control and *Nf2^cKO* P2 livers. **P<0.01 (Mann–Whitney test). Each data point represents an individual cell. Sample size (control, *Nf2^cKO*): P2 (4, 3). (E) Luminal opening in E16.5-E18.5 livers measured as the maximal distance between the apical surface of the ductal plate cell and that of overlying parenchymal cells (lumen diameter, left) as shown (arrow) on representative confocal images (right). *P<0.05 (Student's unpaired t-test). Each data point represents an individual lumen. Sample size (control, *Nf2^cKO*): E16.5 (4, 3), E18.5 (5, 3). (F) Representative confocal images depicting the relationship between moesin+ lumen and Sox9+ cells in biliary structures from control (top left) and *Nf2^cKO* (top right and bottom) P9 livers. Arrowheads indicate moesin+ lumen extending into the parenchyma in *Nf2^cKO*. Asterisks, portal vein. Values shown are mean±s.e.m. Scale bars: 10 µm in D,E; 20 µm in A,F.

involves the formation of luminal surface within regions of cell-cell contact. Examples of this strategy include formation of the zebrafish mechanosensory organ, mammalian blastocoel, salivary gland and pancreatic ductular system (Kesavan et al., 2009; Villasenor et al., 2010; Bedzhov and Zernicka-Goetz, 2014; Durdu et al., 2014; Nedvetsky et al., 2014; Marty-Santos and Cleaver, 2016). In each of these examples the formation of rosette structures, in which all cells are polarized, is driven by apical constriction and precedes the symmetric opening of a lumen at the center of the structure. Our

studies of developing biliary structures in the normal embryo suggest a novel variation of this strategy wherein inductive polarization and lumen expansion initiated by a single cell are synchronized and occur prior to apical constriction (Fig. 7). This more complex strategy requires spatiotemporal coordination of all three activities and accommodates the radial asymmetry inherent to the morphogenetic process.

Our data suggest a model wherein the dramatic amplification of IHBD structures in *Nf2^cKO* livers is initially driven by the
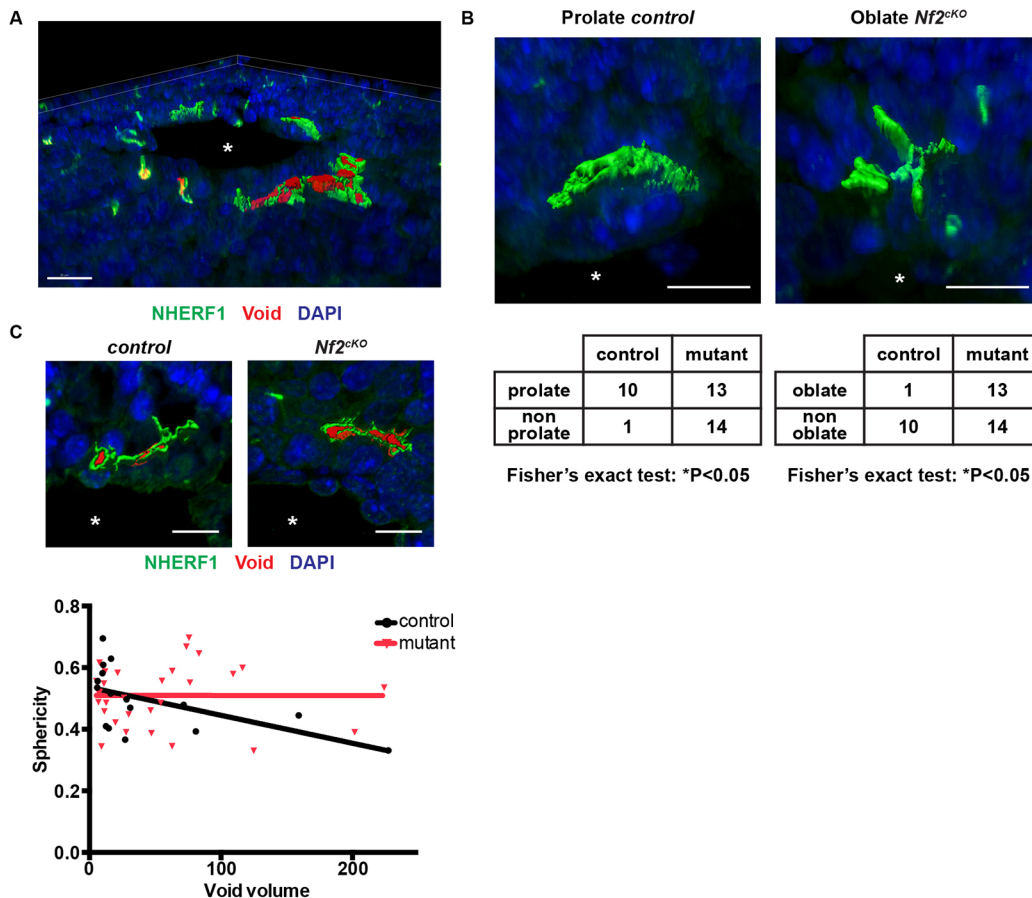
Fig. 6. 3D aspects of developing IHBDs. (A) Representative rendering showing complex 3D architecture of developing control E16.5 livers (from Movie 1). (B) Representative developing prolate (control) and oblate ($Nf2^{cKO}$) lumens labeled with NHERF1 (green), along with their frequencies in E16.5 livers (bottom). Fisher's exact test was used to compare the ratios of prolate:non-prolate or oblate:non-oblate in control versus mutant. (C) Representative luminal cavities (voids, red; top) and graph of sphericity as a function of void volume in control and $Nf2^{cKO}$ E16.5 livers (bottom). Linear regression reveals that sphericity declines as a function of volume in control (*$P<0.05$) but not in $Nf2^{cKO}$ (n.s.). Each data point represents one luminal void volume. Sample size (control, $Nf2^{cKO}$): E16.5 (4, 3). Asterisks, portal vein. Values shown are mean±s.e.m. Scale bars: 20 µm in A; 10 µm in B,C.

hyperextension and opening of *de novo* lumens that progressively recruit neighboring cells to adopt a biliary fate (Fig. 7). *De novo* lumen formation and opening are thought to involve the spatially controlled trafficking of apical material to, and junctional material from, a point of contact between cells, followed by the electrostatic (via the surface presentation of podocalyxin or other charged proteins) (Strilić et al., 2010), osmotic (via aquaporins or other pumps) (Khan et al., 2013) and/or physical (via microvilli) repelling of adjacent apical surfaces to drive lumen opening (Datta et al., 2011). These are all established molecular functions of ERM proteins that could be dysregulated in the absence of NF2 (McClatchey, 2014).

By contrast, the molecular mechanisms that control lumen expansion are not understood. It has recently been shown that the expansion of canalicular lumens within lateral hepatocyte junctions is promoted by increased intercellular stress (Li et al., 2016). Our work suggests that during IHBD morphogenesis lumen expansion is coordinated with apical constriction, a process driven by increased contractility of the medioapical actomyosin cortex and pulling on associated apical junctions (Martin and Goldstein, 2014). We recently found that in the absence of NF2, ERM-driven apical contractility exerts excessive tension on associated cell-cell junctions in 2D cultures of cells derived from adult $Nf2^{cKO}$ neoductular lesions (Chiasson-MacKenzie et al., 2015). Thus, a simple model would be that excessive junctional tension,

exacerbated by ERM-driven lumen opening (Fig. 5E), exaggerates IHBD lumen expansion in the absence of NF2. This would also be consistent with the requirement for ERM activity in expanding strikingly similar *de novo* lumens that drive the 'unzipping' of individual villus structures in the developing gut (Saotome et al., 2004). In the absence of ERM activity, villi fail to unzip completely and the intestinal epithelium aberrantly adopts radially organized rosette-like cystic structures, which could be considered to be the opposite of the *Nf2* mutant biliary phenotype described here. These data support the notion that NF2 and the ERMs work together to control the extent of lumen expansion.

IHBD amplification in the $Nf2^{cKO}$ liver is compounded by the failure of many polarized structures to 'regress', a poorly understood process by which excess structures are eliminated in the normal liver (Zong et al., 2009). Regression does not seem to involve cell death but rather the architectural and transcriptional conversion of cells to a hepatocytic fate. Our study reveals that polarized biliary structures initially form as isolated units and suggests that their subsequent vertical expansion and anastomosis create the mature biliary tubular network. We propose that the failure to anastomose normally triggers regression of polarized biliary structures and the conversion of cells to a hepatocytic fate; the enlargement of these structures in the $Nf2^{cKO}$ liver may promote excess anastomosis and prevent regression. These mechanisms effect significant IHBD amplification in the postnatal
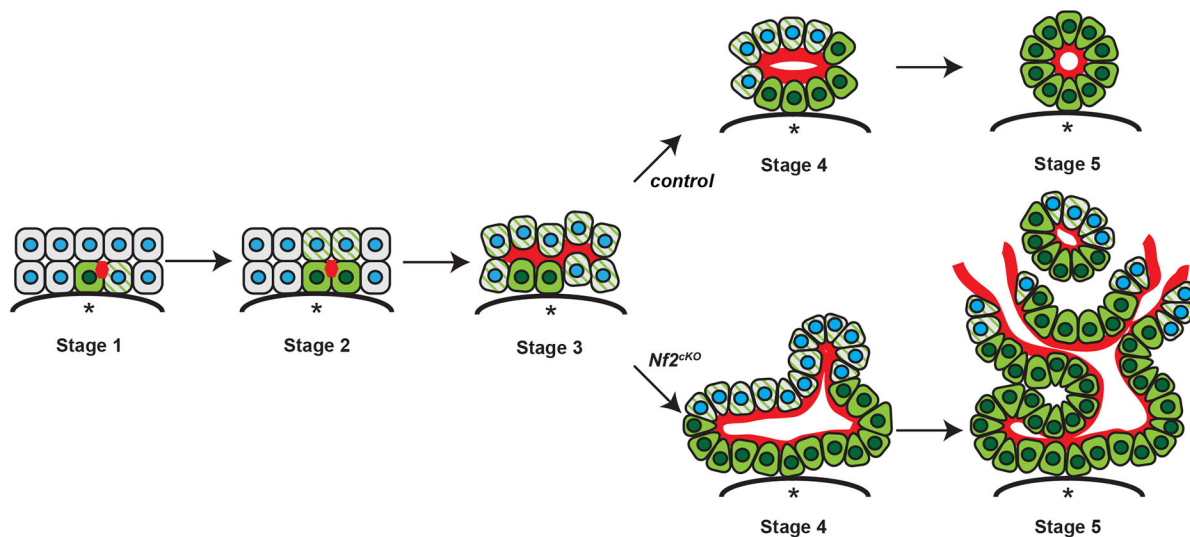
Fig. 7. A novel self-organizing model of IHBD morphogenesis. In the normal embryo, inductive polarization and lumen expansion initiated by a single cell are synchronized and occur prior to apical constriction. By contrast, over-recruitment of biliary cells to developing IHBD structures may occur as a result of failed coordination between lumen expansion and apical constriction in the absence of NF2 (merlin). Red, moesin; green, Sox9; green striped, obligately polarized; blue, nuclei; asterisk, portal vein.

$Nf2^{cKO}$ liver without proliferation; in the adult $Nf2^{cKO}$ liver, cell division further expands the mutant IHBDs and can be blocked by EGFR inhibition (Benhamouche et al., 2010).

A more indirect role for NF2 loss in priming hepatoblasts/ hepatocytes to adopt a biliary fate and/or architecture remains possible. These studies provide an important framework for understanding how downstream events, such as those involving EGFR, TGFβ, Notch and Hippo, all of which can be influenced by NF2 and all of which have been shown to regulate biliary fate and morphogenesis, contribute to the dramatic consequences of NF2 deficiency in the liver (Clotman et al., 2002; Hamaratoglu et al., 2006; Curto et al., 2007; Wilkes et al., 2009; Raynaud et al., 2011; Yimlamai et al., 2014; Pellat et al., 2017; Wu et al., 2017). Indeed, increased ezrin-driven apical polarity in the absence of NF2 could indirectly inactivate Hippo signaling and influence cell fate, as has been proposed in the pre-implantation embryo (Cockburn et al., 2013; Hirate et al., 2013); however, elimination of neither Mst (Hippo) nor Lats (Warts) kinases in the liver phenocopies that of $Nf2$ deficiency. $Mst1/2^{dKO}$ embryos exhibit normal IHBD morphogenesis (Fig. S7) but develop hepatocellular carcinoma as adults, while $Lats^{dKO}$ livers exhibit multilayered biliary structures with no increase in Sox9 expression (Zhou et al., 2009; Lee et al., 2016). Our work sets the stage for a much deeper evaluation of these signaling relationships and will guide the analysis of other proteins that have been implicated in IHBD morphogenesis with the ultimate goal of understanding the fundamental relationship between cell fate and architecture.

The self-organizing nature of IHBD formation and frequent regression of polarized immature IHBD structures underscore the plasticity of architecture and fate exhibited by the two major cell types in the liver. This is consistent with the long-held belief that neoductular lesions are sites of plasticity in the liver (Carpentier et al., 2011) and provides new insight into how that plasticity could be harnessed for regeneration or may underlie disease pathology. For example, strategies to initiate polarization by spatially providing extracellular matrix (ECM) might promote biliary differentiation. Alternatively, ectopic ECM, such as that deposited during fibrosis, might provide an unwanted signal for biliary differentiation in the diseased liver. Importantly, the inductive nature of biliary

morphogenesis suggests that one cell may drive the behavior of others, which could contribute significantly to heterogeneity in biliary tumorigenesis. Our data also suggest that luminal markers such as ERM/NHERF1 might be important early biomarkers of biliary pathology. Finally, defective biliary architecture could spatially dysregulate growth factor signaling. For example, proliferation that begins within neoductular lesions in adult $Nf2^{cKO}$ livers might be prompted by changes in local growth factor availability to which IHBDs are normally insensitive. With this in mind, it is notable that the formation of *de novo* lumen structures in the zebrafish lateral line primordium has been shown to spatially restrict growth factor availability and signaling (Durdu et al., 2014). Our studies of morphogenesis provide a platform for understanding how the self-organizing properties of biliary structures contribute to biliary regeneration and disease.

MATERIALS AND METHODS
Animals

Immunofluorescence
Freshly dissected tissues were fixed in 3.7% formaldehyde in PBS, processed, paraffin embedded and sectioned to 5 μm thickness. Antigen retrieval was performed by boiling in 10 mM citrate buffer (pH 6.0) for 20 min, followed by blocking for 1 h in TBST (50 mM Tris pH 7.4, 300 mM NaCl, 0.05% Tween 20), 1% BSA, 2.5% horse serum. Sections were then incubated overnight at 4°C with the following antibodies: anti-Sox9 (1:100; Millipore AB5535), anti-phospho-histone H3 (1:100; Cell Signaling Technology 9706), anti-Moesin (1:100; clone 38/87, Thermo Fisher MA5-14043; this

antibody recognizes moesin and radixin but not ezrin), anti-E-cadherin (1:500; BD Biosciences 610182), anti-NHERF1 (1:500; Abcam ab3452), anti-HNF4α (1:100; Santa Cruz sc-8987), anti-Par3 (1:100; Millipore 07-330), anti-β-catenin (1:100; BD Biosciences 610154), anti-ZO-1 (1:100; Thermo Fisher 61-7300), anti-aPKC (1:100; C-20, Santa Cruz sc-216), anti-pERM (1:100; Cell Signaling Technology 3141), anti-cleaved caspase 3 (1:100; Cell Signaling 9661) and anti-Ki67 (1:200; BD Pharmingen 556003). This was followed by incubation with Alexa Fluor 488- or 555-conjugated secondary antibodies (1:200; Thermo Fisher) and mounting with Vectashield (Vector Laboratories). Nuclei were stained with DAPI. Confocal images were captured with an LSM 710 inverted laser-scanning confocal microscope (Carl Zeiss) using 40× and 63× oil-immersion objectives.

Transmission electron microscopy
Tissues were fixed in 2% glutaraldehyde in 0.1 M sodium cacodylate buffer (pH 7.2), rinsed and post-fixed in 1% osmium tetroxide in cacodylate buffer. Small tissue pieces were embedded in 2% agarose for ease of handling. Samples were dehydrated and embedded in Epon 812 resin. 1 μm sections were prepared and examined to select representative areas for thin sectioning. Sections were stained with uranyl acetate and lead citrate and examined in a JEOL 1011 electron microscope. Images were captured using an Advanced Microscopy Techniques imaging system.

Image analysis
Fiji software (version 2.0.0) was used for all image processing and analysis (Schindelin et al., 2012). For calculating the number of Sox9$^+$ cells as a function of portal size, lines were drawn across both the long and short axes (diameters) of the portal. All portals exhibiting a long:short axis ratio >1.7 were considered to be in poor cross-section and were excluded from the analysis. The number of Sox9$^+$ cells in the selected region was computed using the analyze particles tool (size range 2 μm to infinity) after adjusting the threshold to resolve individual nuclei. HNF4α$^+$ nuclei and NHERF1$^+$ luminal surface were computed similarly. Normalizations to portal circumference or diameter were calculated after measuring each using the line or freehand tool. Phospho-histone H3 (pH3)$^+$ nuclei, number of polarized structures, and number of cells per polarized structure were all counted manually. The number of polarized structures around a portal was normalized to the short portal axis. Apical and basal widths were measured using the freehand line tool to compute the respective distances between E-cadherin$^+$ junctions. Luminal opening was calculated by drawing a straight line across the longest distance between the NHERF1$^+$ apical surface of the ab-endothelial cell layer to the apical surface of the cell layer on the parenchymal side.

Imaris (Bitplane) and Fiji were used for 3D analysis of luminal architecture. NHERF1 images were inverted in Fiji to identify lumens in proximity to NHERF1$^+$ cells, and the resulting images with labeled lumens were saved as a separate color channel and imported into Imaris along with the corresponding NHERF1 and DAPI image stacks. The surface module of Imaris was used to create 3D surface objects based on image intensity for each channel. The sphericity of the resulting surfaces was computed using the following relation:

$$\Psi = \frac{\pi^{\frac{1}{3}}(6V)^{\frac{2}{3}}}{A},$$

where V is the volume of the object, and A is the surface area. 3D spheroids were fitted to each surface to calculate the prolate and oblate shape index as defined by the following relations:

$$e_{prolate} = \frac{2a^2}{a^2+b^2}\left(1 - \frac{a^2+b^2}{2c^2}\right),$$

$$e_{oblate} = \frac{2b^2}{b^2+c^2}\left(1 - \frac{2a^2}{b^2+c^2}\right),$$

where a, b and c are the magnitudes of the principal axes of the spheroid in order of descending value. Raw data from Imaris 3D rendering are provided in Table S1.

Statistics
Data from all analyses were imported into Prism 6 software (GraphPad) for statistical analysis and plotting of graphs. Results were expressed as mean± s.e.m. Differences between groups were tested using unpaired Student's t-tests and Mann–Whitney tests, as indicated in the figure legends. For the curve-fitting analysis in Fig. S2A, an extra sum of squares F-test was used to establish whether a linear or second-order polynomial function is a better model for the data.

Supplementary information
Supplementary information available online at
http://dev.biologists.org/lookup/doi/10.1242/dev.162123.supplemental

References
Akhurst, B., Croager, E. J., Farley-Roche, C. A., Ong, J. K., Dumble, M. L., Knight, B. and Yeoh, G. C. (2001). A modified choline-deficient, ethionine-supplemented diet protocol effectively induces oval cells in mouse liver. *Hepatology* **34**, 519-522.

Antoniou, A., Raynaud, P., Cordi, S., Zong, Y., Tronche, F., Stanger, B. Z., Jacquemin, P., Pierreux, C. E., Clotman, F. and Lemaigre, F. P. (2009). Intrahepatic bile ducts develop according to a new mode of tubulogenesis regulated by the transcription factor SOX9. *Gastroenterology* **136**, 2325-2333.

Bedzhov, I. and Zernicka-Goetz, M. (2014). Self-organizing properties of mouse pluripotent cells initiate morphogenesis upon implantation. *Cell* **156**, 1032-1044.

Benhamouche, S., Curto, M., Saotome, I., Gladden, A. B., Liu, C. H., Giovannini, M. and McClatchey, A. I. (2010). Nf2/Merlin controls progenitor homeostasis and tumorigenesis in the liver. *Genes Dev.* **24**, 1718-1730.

Bioulac-Sage, P. and Balabaud, C. (2010). Human cirrhosis: monoclonal regenerative nodules derived from hepatic progenitor cells abutting ductular reaction. *Gastroenterol. Clin. Biol.* **34**, 267-269.

Bryant, D. M. and Mostov, K. E. (2008). From cells to organs: building polarized tissue. *Nat. Rev. Mol. Cell Biol.* **9**, 887-901.

Bryant, D. M., Datta, A., Rodríguez-Fraticelli, A. E., Peränen, J., Martín-Belmonte, F. and Mostov, K. E. (2010). A molecular network for de novo generation of the apical surface and lumen. *Nat. Cell Biol.* **12**, 1035-1045.

Carpentier, R., Suñer, R. E., van Hul, N., Kopp, J. L., Beaudry, J.-B., Cordi, S., Antoniou, A., Raynaud, P., Lepreux, S., Jacquemin, P. et al. (2011). Embryonic ductal plate cells give rise to cholangiocytes, periportal hepatocytes, and adult liver progenitor cells. *Gastroenterology* **141**, 1432-1438.

Chiasson-MacKenzie, C., Morris, Z. S., Baca, Q., Morris, B., Coker, J. K., Mirchev, R., Jensen, A. E., Carey, T., Stott, S. L., Golan, D. E. et al. (2015). NF2/Merlin mediates contact-dependent inhibition of EGFR mobility and internalization via cortical actomyosin. *J. Cell Biol.* **211**, 391-405.

Clotman, F., Lannoy, V. J., Reber, M., Cereghini, S., Cassiman, D., Jacquemin, P., Roskams, T., Rousseau, G. G. and Lemaigre, F. P. (2002). The onecut transcription factor HNF6 is required for normal development of the biliary tract. *Development* **129**, 1819-1828.

Cockburn, K., Biechele, S., Garner, J. and Rossant, J. (2013). The Hippo pathway member Nf2 is required for inner cell mass specification. *Curr. Biol.* **23**, 1195-1201.

Curto, M., Cole, B. K., Lallemand, D., Liu, C. H. and McClatchey, A. I. (2007). Contact-dependent inhibition of EGFR signaling by Nf2/Merlin. *J. Cell Biol.* **177**, 893-903.

DEVELOPMENT

Das, T., Safferling, K., Rausch, S., Grabe, N., Boehm, H. and Spatz, J. P. (2015). A molecular mechanotransduction pathway regulates collective migration of epithelial cells. Nat. Cell Biol. 17, 276-287.

Datta, A., Bryant, D. M. and Mostov, K. E. (2011). Molecular regulation of lumen morphogenesis. Curr. Biol. 21, R126-R136.

Desmet, V. J. (2011). Ductal plates in hepatic ductular reactions. Hypothesis and implications. I. Types of ductular reaction reconsidered. Virchows Arch. 458, 251-259.

Durdu, S., Iskar, M., Revenu, C., Schieber, N., Kunze, A., Bork, P., Schwab, Y. and Gilmour, D. (2014). Luminal signalling links cell communication to tissue architecture during organogenesis. Nature 515, 120-124.

Fehon, R. G., McClatchey, A. I. and Bretscher, A. (2010). Organizing the cell cortex: the role of ERM proteins. Nat. Rev. Mol. Cell Biol. 11, 276-287.

Giovannini, M., Robanus-Maandag, E., van der Valk, M., Niwa-Kawakita, M., Abramowski, V., Goutebroze, L., Woodruff, J. M., Berns, A. and Thomas, G. (2000). Conditional biallelic Nf2 mutation in the mouse promotes manifestations of human neurofibromatosis type 2. Genes Dev. 14, 1617-1630.

Gladden, A. B., Hebert, A. M., Schneeberger, E. E. and McClatchey, A. I. (2010). The NF2 tumor suppressor, Merlin, regulates epidermal development through the establishment of a junctional polarity complex. Dev. Cell 19, 727-739.

Hamaratoglu, F., Willecke, M., Kango-Singh, M., Nolo, R., Hyun, E., Tao, C., Jafar-Nejad, H. and Halder, G. (2006). The tumour-suppressor genes NF2/ Merlin and Expanded act through Hippo signalling to regulate cell proliferation and apoptosis. Nat. Cell Biol. 8, 27-36.

Hebert, A. M., DuBoff, B., Casaletto, J. B., Gladden, A. B. and McClatchey, A. I. (2012). Merlin/ERM proteins establish cortical asymmetry and centrosome position. Genes Dev. 26, 2709-2723.

Hirate, Y., Hirahara, S., Inoue, K.-i., Suzuki, A., Alarcon, V. B., Akimoto, K., Hirai, T., Hara, T., Adachi, M., Chida, K. et al. (2013). Polarity-dependent distribution of angiomotin localizes Hippo signaling in preimplantation embryos. Curr. Biol. 23, 1181-1194.

Inaba, M., Sorenson, D. R., Kortus, M., Salzmann, V. and Yamashita, Y. M. (2017). Merlin is required for coordinating proliferation of two stem cell lineages in the Drosophila testis. Sci. Rep. 7, 2502.

Ishibe, S. and Cantley, L. G. (2008). Epithelial-mesenchymal-epithelial cycling in kidney repair. Curr. Opin. Nephrol. Hypertens. 17, 379-385.

Kesavan, G., Sand, F. W., Greiner, T. U., Johansson, J. K., Kobberup, S., Wu, X., Brakebusch, C. and Semb, H. (2009). Cdc42-mediated tubulogenesis controls cell specification. Cell 139, 791-801.

Khan, L. A., Zhang, H., Abraham, N., Sun, L., Fleming, J. T., Buechner, M., Hall, D. H. and Gobel, V. (2013). Intracellular lumen extension requires ERM-1-dependent apical membrane expansion and AQP-8-mediated flux. Nat. Cell Biol. 15, 143-156.

Kopp, J. L., Grompe, M. and Sander, M. (2016). Stem cells versus plasticity in liver and pancreas regeneration. Nat. Cell Biol. 18, 238-245.

Korotkevich, E., Niwayama, R., Courtois, A., Friese, S., Berger, N., Buchholz, F. and Hiiragi, T. (2017). The apical domain is required and sufficient for the first lineage segregation in the mouse embryo. Dev. Cell 40, 235-247 e237.

Lallemand, D., Curto, M., Saotome, I., Giovannini, M. and McClatchey, A. I. (2003). NF2 deficiency promotes tumorigenesis and metastasis by destabilizing adherens junctions. Genes Dev. 17, 1090-1100.

Lee, D.-H., Park, J. O., Kim, T.-S., Kim, S. K., Kim, T.-H., Kim, M.-C., Park, G. S., Kim, J.-H., Kuninaka, S., Olson, E. N. et al. (2016). LATS-YAP/TAZ controls lineage specification by regulating TGFbeta signaling and Hnf4alpha expression during liver development. Nat. Commun. 7, 11961.

Li, Q., Zhang, Y., Pluchon, P., Robens, J., Herr, K., Mercade, M., Thiery, J. P., Yu, H. and Viasnoff, V. (2016). Extracellular matrix scaffolding guides lumen elongation by inducing anisotropic intercellular mechanical tension. Nat. Cell Biol. 18, 311-318.

Macara, I. G. and McCaffrey, L. (2013). Cell polarity in morphogenesis and metastasis. Philos. Trans. R. Soc. Lond. B Biol. Sci. 368, 20130012.

Martin, A. C. and Goldstein, B. (2014). Apical constriction: themes and variations on a cellular mechanism driving morphogenesis. Development 141, 1987-1998.

Marty-Santos, L. and Cleaver, O. (2016). Pdx1 regulates pancreas tubulogenesis and E-cadherin expression. Development 143, 1056.

McClatchey, A. I. (2014). ERM proteins at a glance. J. Cell Sci. 127, 3199-3204.

Mikkola, H. K. and Orkin, S. H. (2006). The journey of developing hematopoietic stem cells. Development 133, 3733-3744.

Muthuswamy, S. K. and Xue, B. (2012). Cell polarity as a regulator of cancer cell behavior plasticity. Annu. Rev. Cell Dev. Biol. 28, 599-625.

Nedvetsky, P. I., Emmerson, E., Finley, J. K., Ettinger, A., Cruz-Pacheco, N., Prochazka, J., Haddox, C. L., Northrup, E., Hodges, C., Mostov, K. E. et al. (2014). Parasympathetic innervation regulates tubulogenesis in the developing salivary gland. Dev. Cell 30, 449-462.

Nelson, W. J. (2009). Remodeling epithelial cell organization: transitions between front-rear and apical-basal polarity. Cold Spring Harb. Perspect. Biol. 1, a000513.

Pellat, A., Vaquero, J. and Fouassier, L. (2017). Role of ErbB/HER family of receptor tyrosine kinases in cholangiocyte biology. Hepatology, doi: 10.1002/hep.29350.

Petrilli, A. M. and Fernández-Valle, C. (2016). Role of Merlin/NF2 inactivation in tumor biology. Oncogene 35, 537-548.

Poncy, A., Antoniou, A., Cordi, S., Pierreux, C. E., Jacquemin, P. and Lemaigre, F. P. (2015). Transcription factors SOX4 and SOX9 cooperatively control development of bile ducts. Dev. Biol. 404, 136-148.

Postic, C. and Magnuson, M. A. (2000). DNA excision in liver by an albumin-Cre transgene occurs progressively with age. Genesis 26, 149-150.

Preisegger, K. H., Factor, V. M., Fuchsbichler, A., Stumptner, C., Denk, H. and Thorgeirsson, S. S. (1999). Atypical ductular proliferation and its inhibition by transforming growth factor beta1 in the 3,5-diethoxycarbonyl-1,4-dihydrocollidine mouse model for chronic alcoholic liver disease. Lab. Invest. 79, 103-109.

Ragkousi, K. and Gibson, M. C. (2014). Cell division and the maintenance of epithelial order. J. Cell Biol. 207, 181-188.

Raynaud, P., Carpentier, R., Antoniou, A. and Lemaigre, F. P. (2011). Biliary differentiation and bile duct morphogenesis in development and disease. Int. J. Biochem. Cell Biol. 43, 245-256.

Richardson, M. M., Jonsson, J. R., Powell, E. E., Brunt, E. M., Neuschwander-Tetri, B. A., Bhathal, P. S., Dixon, J. B., Weltman, M. D., Tilg, H., Moschen, A. R. et al. (2007). Progressive fibrosis in nonalcoholic steatohepatitis: association with altered regeneration and a ductular reaction. Gastroenterology 133, 80-90.

Saotome, I., Curto, M. and McClatchey, A. I. (2004). Ezrin is essential for epithelial organization and villus morphogenesis in the developing intestine. Dev. Cell 6, 855-864.

Schindelin, J., Arganda-Carreras, I., Frise, E., Kaynig, V., Longair, M., Pietzsch, T., Preibisch, S., Rueden, C., Saalfeld, S., Schmid, B. et al. (2012). Fiji: an open-source platform for biological-image analysis. Nat. Methods 9, 676-682.

Sigurbjörnsdóttir, S., Mathew, R. and Leptin, M. (2014). Molecular mechanisms of de novo lumen formation. Nat. Rev. Mol. Cell Biol. 15, 665-676.

Stephenson, R. O., Yamanaka, Y. and Rossant, J. (2010). Disorganized epithelial polarity and excess trophectoderm cell fate in preimplantation embryos lacking E-cadherin. Development 137, 3383-3391.

Strilić, B., Eglinger, J., Krieg, M., Zeeb, M., Axnick, J., Babál, P., Müller, D. J. and Lammert, E. (2010). Electrostatic cell-surface repulsion initiates lumen formation in developing blood vessels. Curr. Biol. 20, 2003-2009.

Takashima, Y., Terada, M., Kawabata, M. and Suzuki, A. (2015). Dynamic three-dimensional morphogenesis of intrahepatic bile ducts in mouse liver development. Hepatology 61, 1003-1011.

Villasenor, A., Chong, D. C., Henkemeyer, M. and Cleaver, O. (2010). Epithelial dynamics of pancreatic branching morphogenesis. Development 137, 4295-4305.

Wilkes, M. C., Repellin, C. E., Hong, M., Bracamonte, M., Penheiter, S. G., Borg, J. P. and Leof, E. B. (2009). Erbin and the NF2 tumor suppressor Merlin cooperatively regulate cell-type-specific activation of PAK2 by TGF-beta. Dev. Cell 16, 433-444.

Wu, N., Nguyen, Q., Wan, Y., Zhou, T., Venter, J., Frampton, G. A., DeMorrow, S., Pan, D., Meng, F., Glaser, S. et al. (2017). The Hippo signaling functions through the Notch signaling to regulate intrahepatic bile duct development in mammals. Lab. Invest. 97, 843-853.

Yimlamai, D., Christodoulou, C., Galli, G. G., Yanger, K., Pepe-Mooney, B., Gurung, B., Shrestha, K., Cahan, P., Stanger, B. Z. and Camargo, F. D. (2014). Hippo pathway activity influences liver cell fate. Cell 157, 1324-1338.

Zhang, N., Bai, H., David, K. K., Dong, J., Zheng, Y., Cai, J., Giovannini, M., Liu, P., Anders, R. A. and Pan, D. (2010). The Merlin/NF2 tumor suppressor functions through the YAP oncoprotein to regulate tissue homeostasis in mammals. Dev. Cell 19, 27-38.

Zhou, D., Conrad, C., Xia, F., Park, J.-S., Payer, B., Yin, Y., Lauwers, G. Y., Thasler, W., Lee, J. T., Avruch, J. et al. (2009). Mst1 and Mst2 maintain hepatocyte quiescence and suppress hepatocellular carcinoma development through inactivation of the Yap1 oncogene. Cancer Cell 16, 425-438.

Zong, Y. and Stanger, B. Z. (2011). Molecular mechanisms of bile duct development. Int. J. Biochem. Cell Biol. 43, 257-264.

Zong, Y., Panikkar, A., Xu, J., Antoniou, A., Raynaud, P., Lemaigre, F. and Stanger, B. Z. (2009). Notch signaling controls liver development by regulating biliary differentiation. Development 136, 1727-1739.